

Article

Aerodynamic Characteristics of Shark Scale-Based Vortex Generators upon Symmetrical Airfoil

S. Arunvinthan¹, V.S. Raatan¹, S. Nadaraja Pillai^{1,*}, Amjad A. Pasha², M. M. Rahman³
and Khalid A. Juhany²

¹ Turbulence and Flow Control Lab, School of Mechanical Engineering, SASTRA Deemed University, Thanjavur, Tamil Nadu 613401, India; sarunvinthan@gmail.com (S.A.); raatan1998@gmail.com (V.S.R.)

² Department of Aerospace Engineering, King Abdulaziz University, Jeddah 21589, Saudi Arabia; aapasha@kau.edu.sa (A.A.P.); khalid@kau.edu.sa (K.A.J.)

³ Physical Science and Engineering Division, King Abdullah University of Science & Technology, Thuwal 23955, Saudi Arabia; Mustafa.Rahman@kaust.edu.sa

* Correspondence: nadarajapillai@mech.sastra.edu; Tel.: +91-9176520125

Abstract: A series of wind tunnel tests were carried out to determine the effect of shark scale-based vortex generators (SSVG) on a NACA 0015 symmetrical airfoil's aerodynamic characteristics. Three different sets of SSVG with varying geometrical parameters, such as chord length, amplitude, and wavelength, were designed and fabricated using 3D printing. The SSVG models were blended to the baseline NACA 0015 symmetrical airfoil. The wind tunnel experiments were performed over the test airfoil mounted with different sets of SSVG at various angles of attack, ranging from 0° to 24° in increments of 3°, and operating in the range of $Re = 2 \times 10^5$. The results revealed that the SSVG blended test airfoil reduced the drag and increased the maximum coefficient of lift (C_{Lmax}), thereby enhancing the overall aerodynamic performance. The SSVG offered noteworthy aerodynamic benefits by effectively altering the flow and causing significant spanwise variation in the flow properties. Additionally, attempts were made to identify the optimum chordwise location to blend the SSVG for effective use.

Keywords: aerodynamic efficiency; airfoils; force balance; shark scale; vortex generators; wind tunnel



Citation: Arunvinthan, S.; Raatan, V.S.; Nadaraja Pillai, S.; Pasha, A.A.; Rahman, M.M.; A. Juhany, K. Aerodynamic Characteristics of Shark Scale-Based Vortex Generators upon Symmetrical Airfoil. *Energies* **2021**, *14*, 1808. <https://doi.org/10.3390/en14071808>

Academic Editors: Steve Burrow and John M. Cimbala

Received: 16 December 2020

Accepted: 18 March 2021

Published: 24 March 2021

Publisher's Note: MDPI stays neutral with regard to jurisdictional claims in published maps and institutional affiliations.



Copyright: © 2021 by the authors. Licensee MDPI, Basel, Switzerland. This article is an open access article distributed under the terms and conditions of the Creative Commons Attribution (CC BY) license (<https://creativecommons.org/licenses/by/4.0/>).

1. Introduction

To overcome the performance degradation caused by flow separation, researchers [1–4] have recently focused their attention on biomimetic devices and systems related to aerodynamics and flow control technologies. The present paper primarily focuses on resolving the flow separation over airfoils, as they have become omnipresent. For instance, airfoils are present in airplane wings, wind turbine blades, propellers, marine rudders, etc. It becomes clear that the airfoil has become one of the integral parts of several human-made engineering structures. However, the flow over the airfoil needs to be attached over the airfoil surface at even greater angles of attack to provide an increased operational capability, efficiency, range, and endurance. An airfoil may adversely experience flow separation, a phenomenon significantly influenced by the airfoil profile's aerodynamic design. Flow control is the method of manipulating or creating the desired boundary layer profile over the object of interest, increasing the lift, decreasing the drag, or delaying the flow separation. Several researchers have stated that flow control over an airfoil is necessary to ensure a better performance [1–5]. Therefore, it becomes clear that flow control technologies have emerged as a promising solution to overcome the poor aerodynamic performance caused by the boundary layer separation on aerofoils' upper surface. Generally, aerodynamic flow control techniques are categorized into active, passive, and hybrid. As the name suggests, the active flow control technique requires additional energy, whereas the passive vortex generators do not require an active energy source. The hybrid flow control technique is

a combination of both active and passive flow control methodologies. Vortex generators are effective aerodynamic flow separation controlling device, and are used to enhance aerodynamic performance. The addition of such passive devices to an airfoil to control the flow under more favorable conditions has been prevalent for decades, whereas the use of biomimetic solutions is limited [6]. One such fascinating study was on utilizing of a shark scale denticular structure as a form of vortex generator over the airfoil. It was observed that the shark skin denticular structure, i.e., small tooth-like structured scales helps sharks move freely through the water with the least resistance. The analogy between the shark scale and the airplane is that they both are designed to freely move through the fluid, whereas the medium is water in terms of the shark, and air in terms of the airplane. Since sharks have existed for the past 55 million years, Bar-Cohen [7] expressed that nature has exerted strong pressure by evolution on shark features, thereby making them potentially optimal to move quickly through the water. It was further confirmed that the short fin mako shark (*Isurus paucus*) is one of the fastest and most agile sharks, capable of maintaining speeds of over 20 m/s for a short interval of time [8–10]. An adult short fin mako can grow up to 4.3 m in length, and because of its huge size, the sharks must depend upon their intrinsic speed and the level of activity to hunt down their prey. Moreover, the shark's scales, i.e., the denticular structure on its skin, are presumed to be used for flow control and/or drag reduction. Several studies on shark scales have emerged recently, intending to use them for aerial drones, uncrewed aerial vehicles (UAVs), microaerial vehicles (MAVs), and wind turbines, to make them more aerodynamically efficient. Lang et al. [11] morphologically investigated such shark scales' three-dimensional geometry using a scanning electron microscope (SEM). They found that these identical denticular structures are oriented in rows varying in size from the head to the shark's tail and measuring approximately 0.2 mm in length. Motta et al. [12] found that the shark scale's bristling angle can vary up to a maximum of 50°. It was reported that the shark scales can erect at an angle called the bristling angle (β) when it experiences a reverse flow. A schematic representation of individual shark scales under both the bristled and non-bristled conditions is shown in Figure 1.

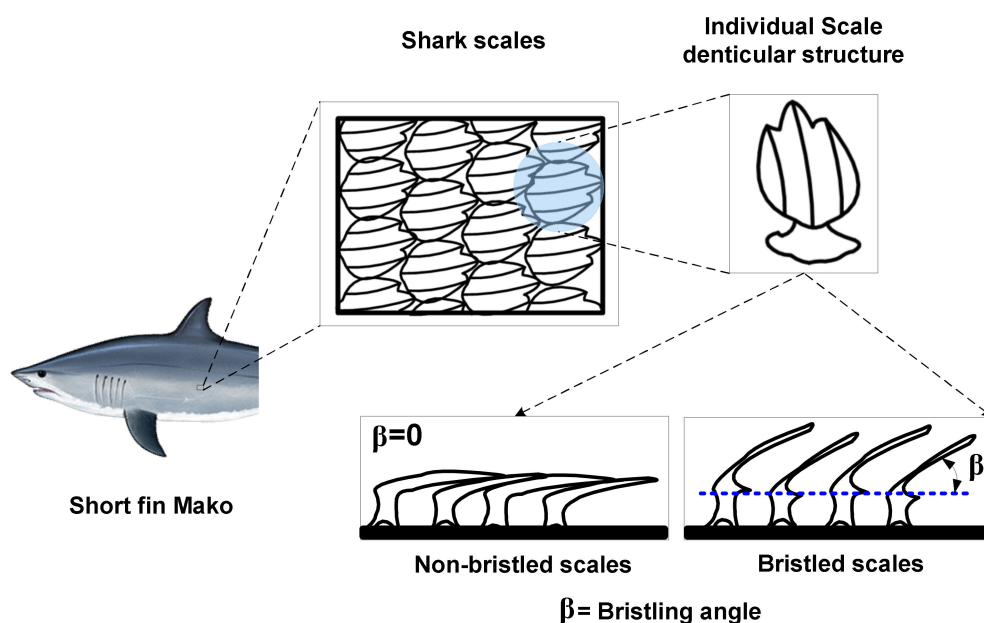


Figure 1. A schematic representation of scales on the short fin mako sharks and denticular structure of individual scales under bristled and non-bristled condition.

Lang et al. [13] studied the sharkskin's flow at normal swimming speeds and claimed that these bristled scales provide local separation control, thereby helping the shark move

faster in the water with the least drag. Bechert et al. [14] experimentally investigated the drag present over the sharkskin and reported that a non-bristled shark scale could provide up to 3% drag reduction. Furthermore, it was also suggested that the shark scales could act as vortex generators. These shark scales induce enhanced mixing between the scales, leading to a reduction in boundary layer separation over the surface, thereby ensuring that the flow remains attached to the surface for an extended period. Therefore, from the literature, it becomes clear that shark scales tend to impede body's separation by providing local flow separation control. Following that, researchers started using shark skin resembling surfaces on engineered structures to reduce drag. Lang et al. [15] experimented on a baseline smooth PVC cylinder and a modified shark scale skinned PVC cylinder. With airfoils becoming omnipresent, researchers have started focusing on airfoils, since they are integral parts of aircraft, UAVs, MAVs, and many other engineering structures, like propellers, wind turbine blades, etc. Table 1. Illustrates various flow control techniques studied by researchers. Even though research work on the airfoil and its flow control mechanisms has been carried out for the past few decades, the problem still persists, and vortex generators remain a simple yet effective way to maintain a favorable lift to drag ratio [16–18]. Henceforth, in this paper, the effectiveness of utilizing shark scale-based bio-inspired vortex generators (SSVG) upon the NACA 0015 test airfoil was experimentally investigated in detail.

Table 1. Flow control techniques.

Methodology	Categorization	Reference
Vortex generators	Passive	Fouatih et al. [19], Wang et al. [20]
Suction	Active	Zhi-yong et al. [21], Yousefi et al. [22]
Synthetic jets	Active	You et al. [23], Minelli et al. [24]
Periodic excitation	Active	Greenblatt et al. [25], Brunn et al. [26]
Blowing	Active	Yousefi et al. [27], Ganesh et al. [28],
Surface wrinkling	Passive	Raayai-Ardakani et al. [29]
Riblets	Passive	Raayai-Ardakani et al. [30], Zhang et al. [31]
Morphing/geometrical profile modification	Passive	Ismail et al. [32], Jones et al. [33]
Spanwise groove	Passive	Luo et al. [34], Law et al. [35]
Grooves	Passive	Seo et al. [36], Mu et al. [37]
Surface modification	Passive	McAuliffe et al. [38], D'Allesandro [39]
Indents/ surface treatments	Passive	Robarge et al. [40]
Blowing and suction	Hybrid	Huang et al. [41], Junxuan et al. [42]
Plasma	Active	Akansu et al. [43], Guoqiang et al. [44]
Leading-edge protuberances	Passive	Arunvinthan et al. [45], Zhanget al. [46]

The paper is organized as follows. Section 2 deals with the experimental methodology discussing in detail the synthesis of the experimental setup and the equipment involved in the measurements. Following this, the influence of shark scale-based bio-inspired vortex generators (SSVG) on the airfoils' aerodynamic characteristics is discussed in detail in Section 3. The conclusions are presented in Section 4.

2. Experimental Methodology

All the experiments performed in this study were carried out in a low-speed subsonic wind tunnel facility located at SASTRA deemed university. The wind tunnel has a rectangular test section of $300 \times 300 \times 1500$ mm cross-section, with a maximum velocity of 60 m/s. The free-stream turbulence intensity of the wind tunnel is 0.51%. In this study, the mean free-stream velocity was fixed at 30 m/s, corresponding to a Reynolds number (Re) of 2.0×10^5 for all the test cases. Three different sets of shark scale geometries, varying in chord length, span, amplitude (A), and wavelength (λ) were designed and fabricated using a 3D printing methodology at an accuracy of $100 \mu\text{m}$ using polylactide (PLA) material. The labels and geometric specifications of the SSVG's are listed in Table 2. Likewise, a rectangular vortex generator of length = 10 mm and height = 6 mm was also experimentally investigated to compare the aerodynamic characteristics of a bio-inspired SSVG against the conventional VG. A schematic representation of the baseline clean wing, conventional rectangular vortex generator and modified SSVG blended test models are presented in Figure 2. Figure 3 shows the real-time test models blended with 3D-Printed SSVG. As we knew that the efficiency of the vortex generators greatly depends upon the chordwise position, the present study investigated the effectiveness of SSVG at three different chordwise locations, namely $0.3C$, $0.5C$, and $0.8C$, respectively. In the present study, the SSVG was blended with the airfoil's surface at a bristling angle of $\beta = 0^\circ$. The same airfoil was used, over which different sets of SSVG's were blended to preserve the mean chord length and span of the baseline model.

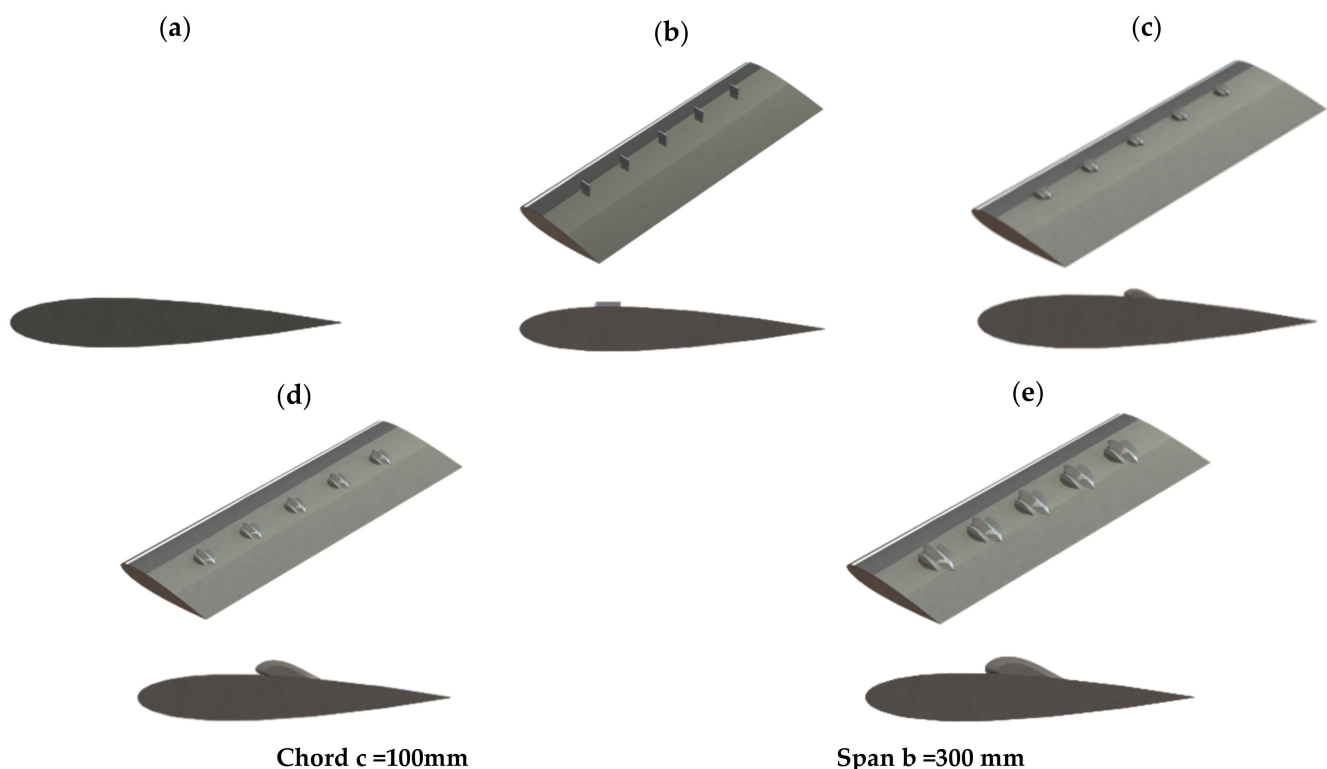


Figure 2. A schematic representation of test models: (a) baseline clean wing, (b) conventional rectangular vortex generator (VG), (c) 5S type shark scale vortex generators (SSVG), (d) 5M type SSVG, and (e) 5L type SSVG.

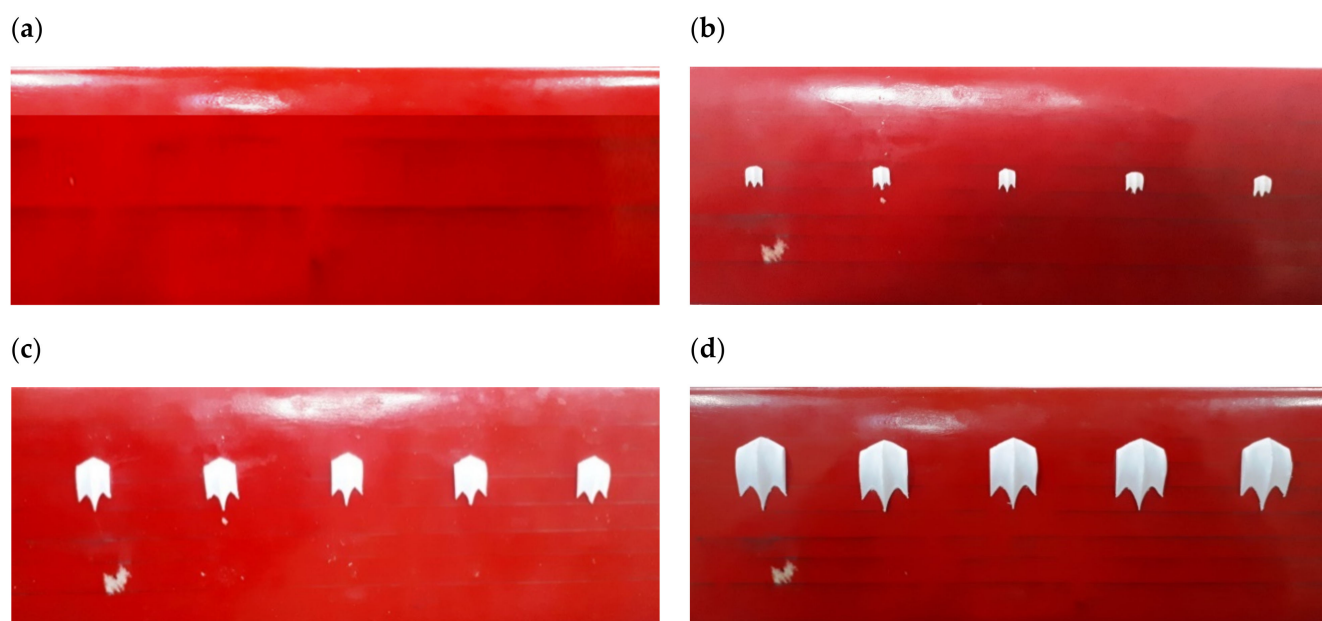


Figure 3. Photographs of baseline and modified wing model with shark scale vortex generator (SSVG): (a) baseline clean wing, (b) 5S type SSVG, (c) 5M type SSVG, and (d) 5L type SSVG.

The test airfoil considered in this study was a NACA 0015 symmetrical airfoil with a 15% thickness to chord ratio. The test airfoil model had a mean chord length of $c = 100$ mm and span $b = 300$ mm. The rectangular test airfoil model was carved out of wood using CNC and then post-processed to obtain an ultra-smooth fine texture. To study the influence of bio-inspired shark scale vortex generators on the airfoil's aerodynamic characteristics, 3D printed shark scales were blended to the test airfoil at various chordwise locations and tested. A typical representation of the three different sets of shark scale models considered in this study is depicted in Figure 3. The leading-edge amplitude (A) and wavelength (λ) of these three different sets of shark scales changes, and their corresponding values are also presented in Table 2.

Table 2. Label and dimensions of the test models.

Label	Chord (mm)	Span (mm)	Amplitude (A) (in mm)	Wavelength (λ) (in mm)
5S	10	6	2	3
5M	20	12	3	6
5L	30	18	4	9

To ensure the reliability of the data acquired from the wind tunnel, its horizontal and vertical velocity profiles were thoroughly measured using a Pitot tube attached to an MPS 4264 simultaneous pressure scanner of M/s Scanivalve with a sampling frequency of 700 Hz at 10,000 data samples. It was found that the tunnel wall boundary layer covered 8.2% of the model span at the operating Reynolds number range. Based on the suggestions from the previous framework [47], it is known that when the tunnel boundary layer covers less than 10% of the model span, then the effect of the tunnel-wall boundary layer on the aerodynamic force measurement is minimal. A schematic representation of individual SSVG along with their corresponding dimensions and 3D printed SSVG models are presented in Figure 4. It also shows the typical representation of the SSVG blended over test airfoil model and its orientation towards the oncoming freestream flow to provide better understanding for the readers.

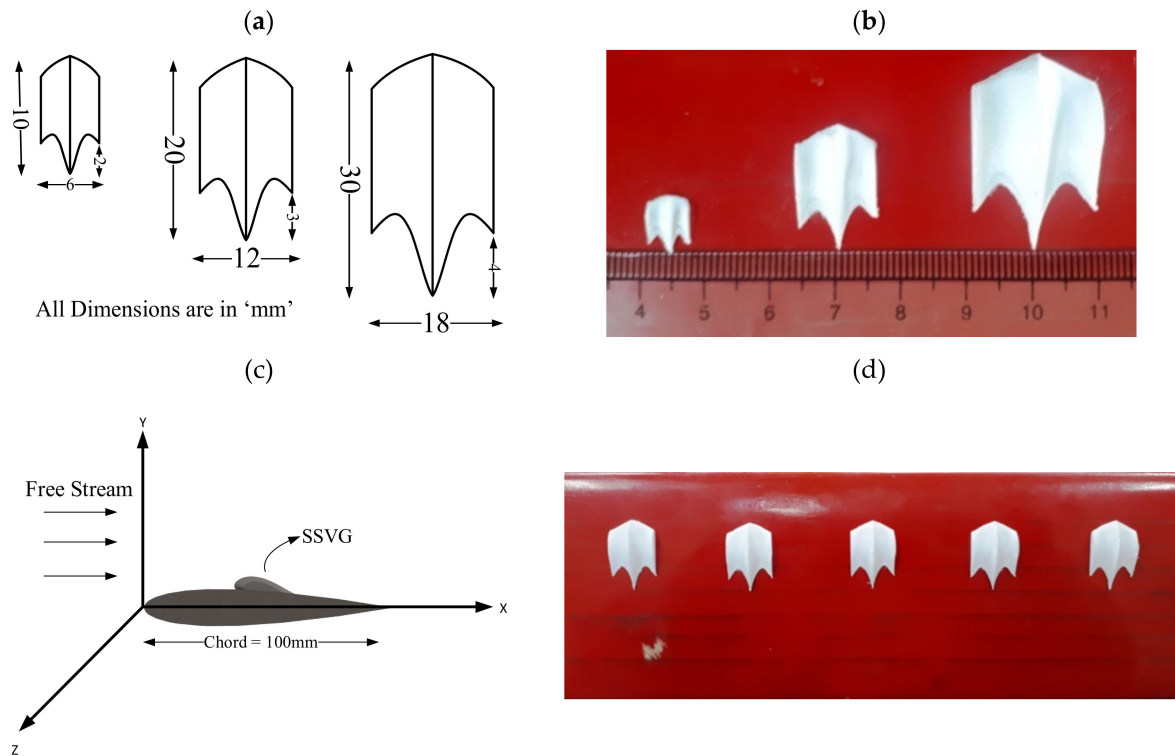


Figure 4. Shark scale vortex generator (SSVG): (a) Individual Shark Scale Vortex generator (SSVG) models, (b) 3D Printed SSVG models, (c) Schematic representation of the SSVG blended over the test airfoil, and (d) A typical view of the SSVG blended over the test airfoil.

A calibrated three-component force balance set up was utilized in this study to measure the aerodynamic forces acting on the test models. The load cells were capable of measuring forces up to ± 98.06 N in streamwise, vertical, and transverse directions. The test models were then mounted onto the load cell using rectangular clamp plates affixed with a hole designed to effectively restrict the axis of rotation and transfer the forces directly to the load cell. The load cell setup was mounted directly below the tunnel test section so that the test model could be directly mounted, as shown in Figures 5 and 6, respectively. The measurements obtained from the load cell setup were the total lift force (F_L) and the drag force (F_D) in (kg). The coefficient of lift (C_L) and coefficient of drag (C_D) could be obtained from the F_L and F_D using the free stream dynamic pressure and the planform area of the test airfoil [48–51]. The coefficient of lift (C_L) and coefficient of drag (C_D) were calculated as illustrated in [52] by the following formulae:

$$C_D = F_D / 0.5\rho v^2 s \quad (1)$$

$$C_L = F_L / 0.5\rho v^2 s \quad (2)$$

Here, ρ is the freestream density in kg/m^3 , v is the freestream velocity in m/s , and s is the airfoil span in m^2 .

Generally, the uncertainties involved in the wind tunnel experiments were either due to the geometrical uncertainty of the models or due to the instruments involved. In this present study, all the test models were repeatedly measured using digital vernier calipers at multiple locations to ensure their dimensions. The maximum error (%) was identified as 3.17, which is relatively low. The other uncertainties involved in the experiments included an angle of attack positioning error ($\pm 1^\circ$ Manual error) and a force balance instrument error. The three-component force balance setup utilized in this experiment had a tolerance of $\pm 0.08\%$, and the scanivalve pressure scanner accounted for $\pm 0.06\%$ uncertainty. Since

many precise instruments were involved in this experimental setup, incorporating the correction factors would influence only the third and fourth decimal of the aerodynamic force coefficients. For instance, the lift coefficient (C_L) for 5S @ 0.8C was 0.66, and the value became 0.660924 when the correction factors were implemented. Therefore it becomes clear that the measurements did not encounter any serious uncertainty effect.

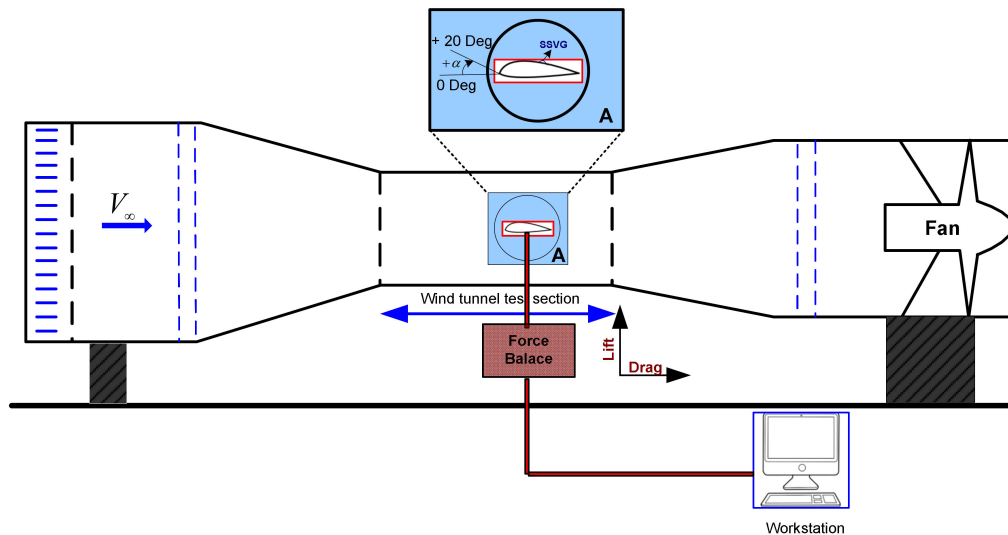


Figure 5. Schematic of the low-speed subsonic wind tunnel facility located at SASTRA Deemed university.



Figure 6. Test airfoil mounted to the three-component force balance setup.

3. Results

The measured aerodynamic force coefficients, coefficient of lift (C_L), coefficient of drag (C_D), obtained for the three different SSVG configurations, namely 5S, 5M, and 5L, at other chordwise locations at various angles of attack (α) varying in the range of 0° – 24° with an increment of 3° and operating at $Re=2.0 \times 10^5$ are discussed in detail in this section. Furthermore, the aerodynamic characteristics of the bio-inspired SSVG were compared against the aerodynamic coefficients of the baseline clean wing configuration and the wing was blended with conventional rectangular vortex generator configurations to get a detailed insight.

3.1. Influence of SSVG on the Aerodynamic Characteristics of the Baseline Model

The effect of the bio-inspired SSVG on the aerodynamic forces like the coefficient of lift (C_L) and coefficient of drag (C_D) for the clean baseline wing and the modified model blended with conventional rectangular VG and bio-inspired SSVG is shown in Figures 7 and 8, respectively. It was observed that that the aerodynamic forces over the baseline and the modified models blended with vortex generators were appreciably different. The

coefficient of lift (C_L) for the baseline clean wing model increased with the increase in the angle of attack (α) till $\alpha = 9^\circ$, and thereby reaches a maximum lift coefficient ($C_{L_{\max}}$) of 0.64. However, the C_L for the modified wing model blended with SSVG followed the same trend line as the baseline model till $\alpha = 9^\circ$, but it continued to produce lift till $\alpha = 12^\circ$, exhibiting significant delay stall characteristics. In addition to the stall delay characteristics, the modified model blended with the SSVG showed an increase in the maximum lift coefficient ($C_{L_{\max}}$). Figure 7 shows that the modified wing model blended with SSVG exhibited a maximum lift coefficient ($C_{L_{\max}}$) of 0.66 at $\alpha = 12^\circ$, which is higher than the maximum C_L of the baseline clean wing configuration. Therefore, based on the results, it can be reported that the modified model with SSVG exhibited stall delay characteristics associated with aerodynamic performance enhancement. Similarly, the aerodynamic characteristics of the conventional rectangular vortex generators are also compared with the results of the baseline clean wing configuration and the bio-inspired SSVG in Figure 7. The results indicate that the lift curve of the modified wing model blended with a conventional rectangular vortex generator was quasi-linear. From Figure 7, it can be inferred that the conventional rectangular vortex generator showed a maximum lift coefficient ($C_{L_{\max}}$) of 0.54. Even though the effect of the conventional rectangular vortex generator on the aerodynamic characteristics was detrimental, the effect of the rectangular VG was visible on the delayed separation characteristics, i.e., the stall occurred at $\alpha = 12^\circ$ relative to $\alpha = 9^\circ$ of the baseline clean wing configuration. This result is in good agreement with previous studies and coincides with the work [19]. Correspondingly, when the vortex generators could not maintain an attached flow over the airfoil at high angles of attack (in this case, of beyond $\alpha = 12^\circ$), a sudden drop in the lift coefficient appeared, indicating the stall phenomenon. However, in the post-stall angles, the aerodynamic characteristics of both the baseline clean wing configuration and the modified models blended with rectangular VG and SSVG were almost the same. It is observed from Figure 7 that the lift curve characteristics of all three cases were almost consistent; between $15^\circ < \alpha < 24^\circ$. The maximum lift coefficient ($C_{L_{\max}}$) of the modified wing blended with SSVG showed a 3.80% and 18.37% increase relative to the baseline clean wing configuration and the modified wing model blended with conventional rectangular vortex generators, respectively. Furthermore, the lift curve slope ($dC_L/d\alpha$) indicated that the hard stall characteristics were common to all the models, whereas the stall angle was delayed by 3° with the use of vortex generators for both the rectangular VG and SSVG. It is noteworthy that the modified model blended with SSVG outperformed the conventional rectangular VG configuration in terms of maximum lift coefficient ($C_{L_{\max}}$). Therefore, based on the experimental results, it can be concluded that at $Re = 2.0 \times 10^5$, the modified wing model blended with SSVG outperformed the conventional rectangular VG and baseline clean wing configuration by offering unique aerodynamic benefits, like a delayed stall angle of 3° associated with an increase in the maximum lift coefficient ($C_{L_{\max}}$) by 18.37% when compared against the modified wing model blended with conventional rectangular VG rendering the SSVG advantageous in terms of both aerodynamic performance and stall delay characteristics.

Figure 8 illustrates the variation of coefficient of drag (C_D) with the angle of attack (α) for all the three test models at various angles of attack (α) ranging from 0° to 24° in increments of 3° at $Re = 2.0 \times 10^5$. The drag coefficient did not exhibit any significant changes at lower angles of attack (α), however as the angle of attack increased, the drag coefficient (C_D) increased, and this behavior became more important near the vicinity of the stall region of the airfoil. Figure 8 shows that for the baseline wing configuration, the coefficient of drag (C_D) exhibits a sudden rise at $\alpha = 9^\circ$, corresponding to stall, following which the C_D continued to increase at a slower rate till $\alpha = 18^\circ$. It is of interest that little difference was present in the modified wing model's drag characteristic curves blended with conventional rectangular VG relative to the baseline clean wing configuration. When the angle of attack was at $\alpha = 9^\circ$, a precipitous increase in drag coefficient occurred in the case of the modified wing model blended with conventional rectangular VG, as the control device produced a disturbance on the upper surface of the profile. More precisely,

the disturbance induced by the intensity of the vortices generated from the rectangular VGs was considered as the plausible reason behind the increase in the drag coefficient for the modified wing model blended with the conventional rectangular vortex generator. Therefore, based on these results, it can be reported that the modified wing model blended with conventional rectangular VGs offered a stall delay benefit, with a slight drag penalty resulting from the induced friction produced by the adopted vortex generator, for most of the angles of attack ranging between $9^\circ < \alpha < 24^\circ$ in the test range. On the other hand, the presence of the SSVG managed to produce a smooth rise in the coefficient of drag (C_D), associated with an increase in the maximum lift coefficient (C_{Lmax}). It can be seen from Figure 8 that the drag curves of the modified model with SSVG showed a linear increase in the coefficient of drag (C_D) throughout the test range, except between the $18^\circ < \alpha < 21^\circ$ angles of attack (α). In contrast to the baseline clean wing configuration and the modified wing model blended with conventional rectangular VG, there was no sudden increase in the coefficient of drag (C_D) associated with the stall in the modified model blended with SSVG. The drag coefficient (C_D) of the modified wing model blended with SSVG was significantly lower than its equivalent counterpart (i.e., the modified wing model blended with conventional rectangular vortex generators) throughout the entire test range, except between $0^\circ < \alpha < 6^\circ$. This increase in the drag coefficient for the modified model blended with SSVG is believed to be caused by the increase in the skin friction and the pressure drag attributed to the attachment of the SSVG over the airfoil surface. At the same time, it is also evident from Figure 8 that the modified wing model blended with SSVG exhibited the lowest drag coefficient of all the test models, including the baseline clean wing configuration in the post-stall region between $12^\circ < \alpha < 18^\circ$. However, at the remaining angles of attack, the drag coefficient of the modified models blended with SSVG was higher than the baseline clean wing configuration. Although the drag coefficient (C_D) of the modified model blended with SSVG was relatively greater than the baseline clean wing model, it was substantially lower than the drag coefficient (C_D) of the modified model blended with the conventional rectangular VG. Therefore, the modified model blended with SSVG proved to be the most practical planform geometry for future applications requiring stall delay characteristics in addition to increased maximum lift coefficient (C_{Lmax}). Furthermore, attempts were made to identify the optimum size of the SSVG, along with the chordwise location (x/C) at which the SSVGs can be blended with the wing section. In this study, three different sets of SSVGs, each blended at three different chordwise locations 0.3, 0.5, and 0.8C, as shown in Figure 9 were investigated in detail. The corresponding aerodynamic lift and drag forces were measured using the force measurements obtained from the wind tunnel, and the results are discussed in detail in the upcoming sections of the paper.

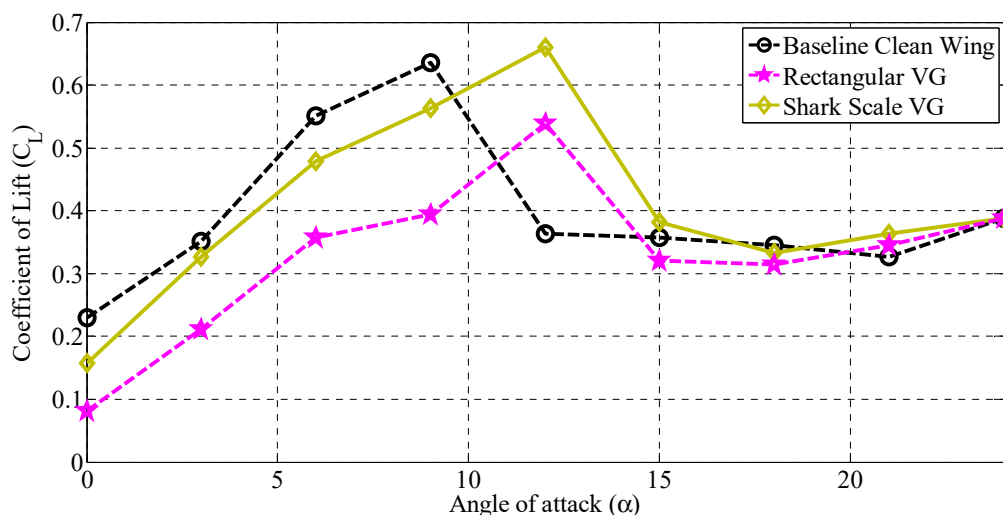


Figure 7. Coefficient of lift (C_L) vs. angle of attack (α) for baseline and modified model with shark scale vortex generators (SSVG).

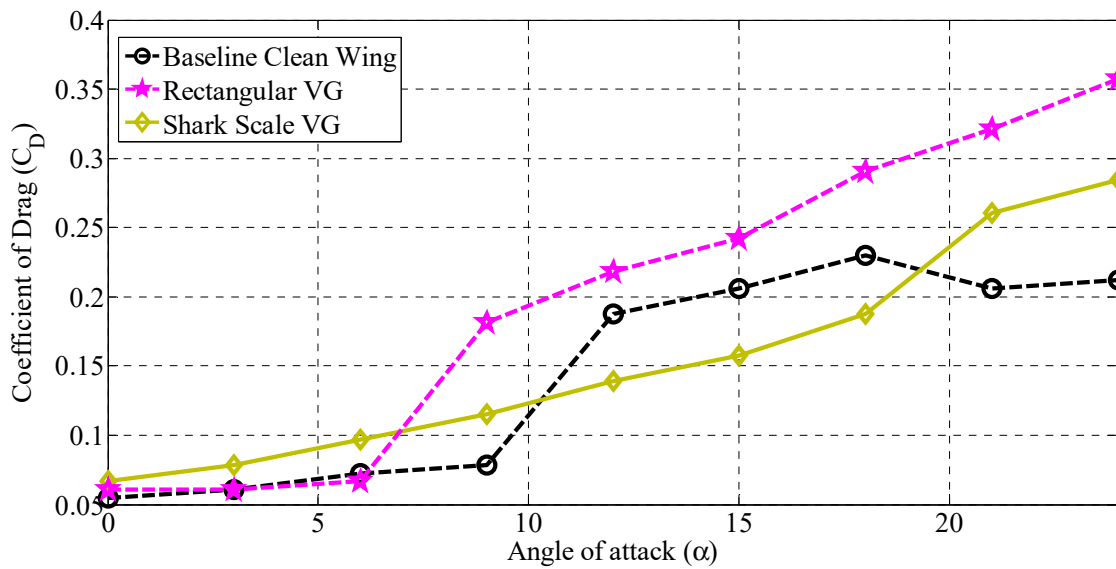


Figure 8. Coefficient of drag (C_D) with the angle of attack (α) for baseline and modified model with SSVG.

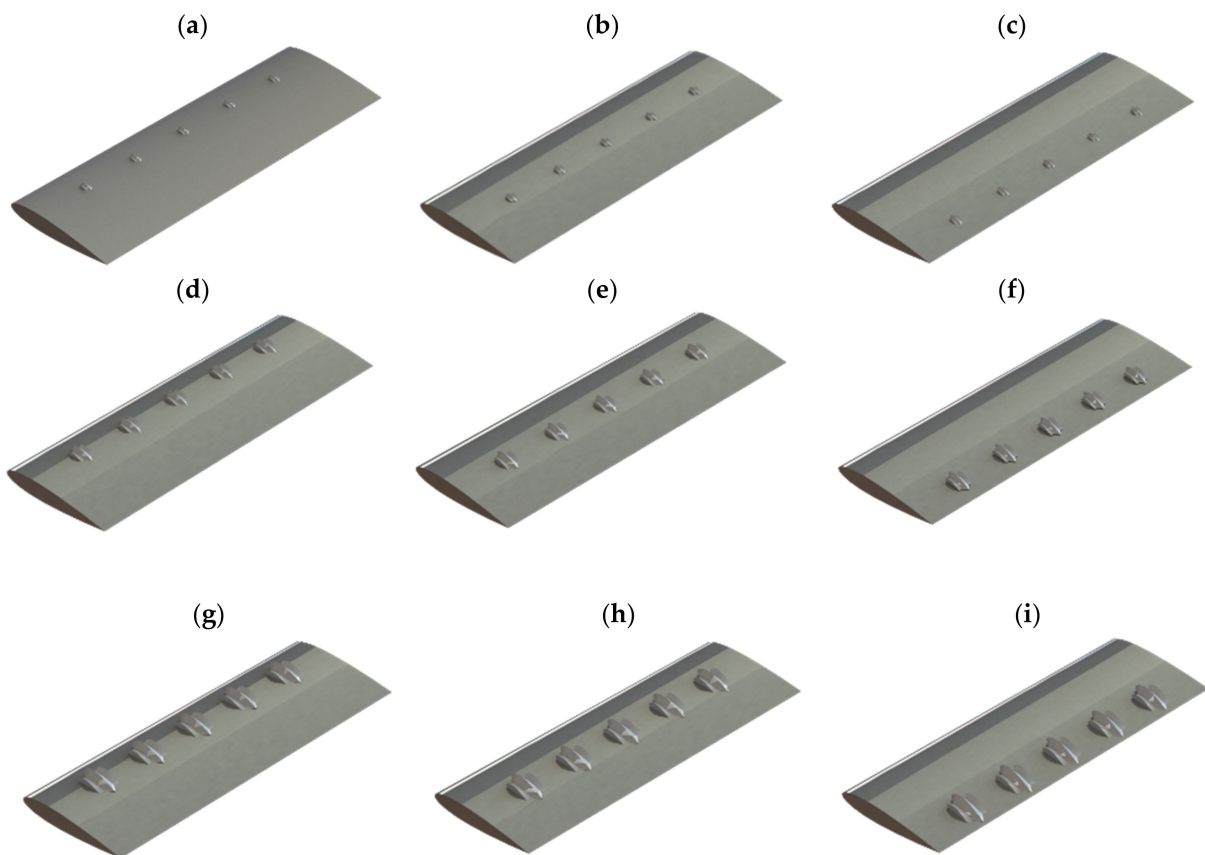


Figure 9. A schematic representation of 5S type SSVG (a–c), 5M type SSVG (d–f), and 5L type SSVG (g–i) blended over the test airfoil at various chordwise locations.

3.2. Influence of 5S Type SSVG at Various Chordwise Locations (x/C)

The variation of characteristic lift coefficient (C_L) vs. angle of attack (α) for the baseline clean wing configuration, modified wing model with conventional vortex generators, and the modified model with 5S type SSVG located at three different chordwise locations (x/C) is shown in Figure 10. For all the test models, the coefficient of lift (C_L) increased linearly with the angle of attack (α) in the pre-stall regime, followed by hard-stall characteristics

(i.e., sudden loss of lift) at the stall point. However, in the baseline clean wing configuration the model stalled between $9^\circ < \alpha < 12^\circ$, whereas in the case of the modified model blended with conventional rectangular VG and 5S type SSVG, the stall occurred between $12^\circ < \alpha < 15^\circ$, except 5S @ 0.3c. Of the three different sets of SSVG, the coefficient of lift (C_L) of 5S @ 0.3C was comparatively low compared to its counterparts and the baseline clean wing model. At the same time, beyond the baseline stall angle of attack $\alpha = 9^\circ$, 5S @ 0.8C continued to produce greater lift around 3.80% accompanied by a delay in the stall angle by 3° . The increased coefficient of lift (C_L) and the delayed stall angle can be attributed to the modification of the spanwise flow pattern induced by the SSVG. In the case of 5S @ 0.5C, even though the model continued to produce lift beyond the baseline stall angle and offer stall delay benefit, the overall maximum lift coefficient (C_{Lmax}) was relatively low when compared against the 5S @ 0.8C type SSVG configuration. Similarly, in the post-stall region, the 5S @ 0.3C and 5S @ 0.8C type SSVG configuration exhibited better aerodynamic performance enhancement in terms of lift characteristics for a wide range of angles of attack (α), ranging between $15^\circ < \alpha < 24^\circ$, except at $\alpha = 18^\circ$. Based on these results, it can be reported that the modified model blended with 5S type SSVG located at 0.5C and 0.8C outperformed the baseline clean wing configuration in the post-stall region. However, at the same time it should be noted that the modified model with SSVG 5S @ 0.3C did not provide any significant aerodynamic benefit in terms of both the coefficient of lift (C_L) and stall delay, under both the pre-stall and post-stall conditions. It is worth noting that the modified model blended with 5S type SSVG (5S @ 0.5C and 5S @ 0.8C) showed better lift characteristics than its equivalent counterpart (i.e., modified wing model blended with conventional rectangular VG).

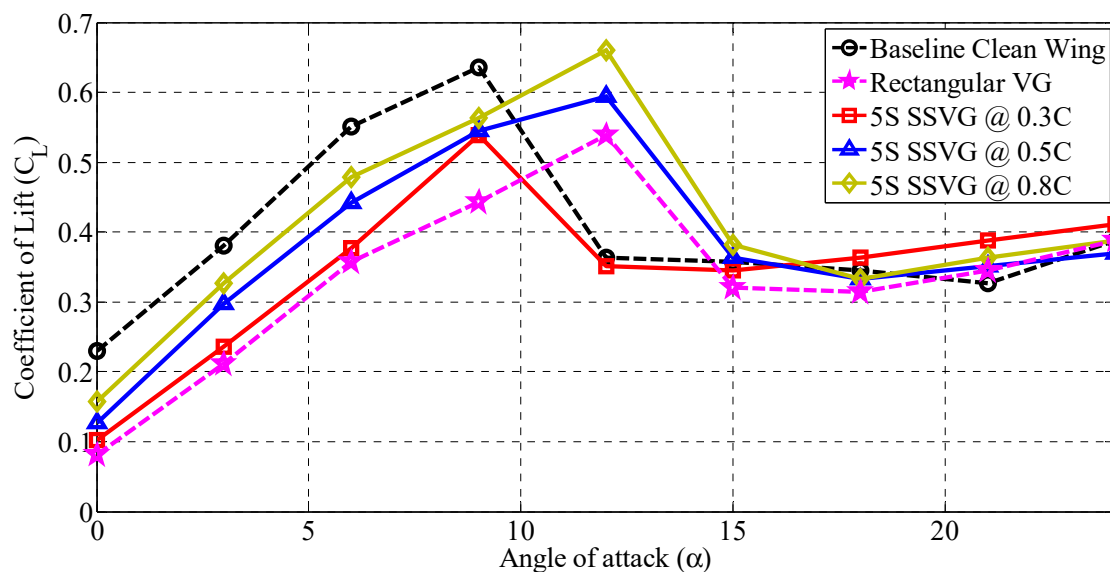


Figure 10. Coefficient of lift (C_L) vs. angle of attack (α) for the baseline and modified model with Scheme (5S) SSVG.

The drag coefficients (C_D) of the baseline clean wing configuration, modified wing model blended with conventional rectangular VGs, and the modified models with 5S type SSVG fixed at various chordwise locations were compared against the angle of attack (α), as shown in Figure 11. It is shown in Figure 11 that the drag coefficient (C_D) increased with the increase in the angle of attack (α) for all the test models. However, an increase in the drag coefficient (C_D) of the modified model blended with 5S type SSVG (5S @ 0.5C and 5S @ 0.8C) relative to the baseline clean wing configuration and the modified model blended with conventional rectangular VG was apparent over the pre-stall angles ranging between $0^\circ < \alpha < 9^\circ$. Both the 5S @ 0.5C and 5S @ 0.8C SSVG led to an increased drag coefficient and a reduced angle at which the drag curves for these models departed from the baseline curve. The stall was visible in the (C_D) curve for the baseline model accompanied by a

sudden rise, and on the other hand, the coefficient of drag (C_D) of the modified models instead continued to increase slowly. Moreover, it should, however, be noted that the modified model blended with conventional rectangular VG showed a rapid rise in the drag coefficient at $\alpha = 9^\circ$. Following this, the modified model blended with conventional rectangular VG continued to exhibit the largest drag coefficient (C_D) out of all the test models over the entire angle of attack range considered. It is visible from the data shown in Figure 11 that neither the baseline clean wing model nor the modified model blended with 5S type SSVG exhibited drag coefficients (C_D) that were greater than the modified wing model blended with conventional rectangular VG between $9^\circ < \alpha < 24^\circ$. Therefore, it becomes clear that the modified models blended with 5S type SSVG showed relatively less drag when compared against the baseline clean wing configuration, and the modified model blended with conventional rectangular VG at post-stall angles. This is because the separated shear layer generated from the SSVG imparted momentum to the flow adjacent to the surface, and thereby contributed to the increased maximum coefficient of lift (C_{Lmax}). In other words, the separated turbulent boundary layer from the SSVG helped re-energize the flow, thereby offering better stall delay characteristics by effectively mitigating the flow separation at higher angles of attack (α). However, at lower angles of attack (α) the modified models with SSVG showed an increased drag coefficient, which was most likely due to the increase in pressure over the suction side of the airfoil induced by the SSVG (i.e., the increase in pressure due to the disturbance caused by the SSVG to the flow moving over the upper surface of the airfoil). In the pre-stall region, the separated shear layer arising out of the SSVG increased the pressure on the suction side of the surface of the airfoil, resulting in a sharp decline in the favorable pressure gradient. The decline in the favorable pressure gradient caused a loss of lift in the pre-stall angles. It is also evident from Figure 10 that in the pre-stall angles, the modified model with 5S type SSVG exhibited a lesser lift coefficient (C_L) than the baseline model. Hence, a pressure model could be utilized in the future to gain a more detailed insight into the surface pressure alterations induced by the SSVG.

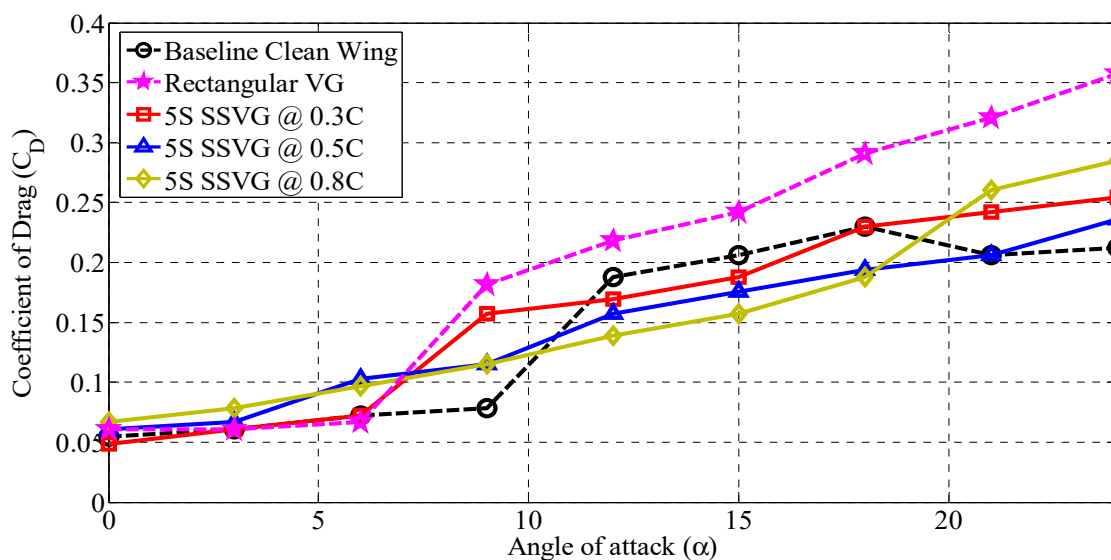


Figure 11. Coefficient of drag (C_D) vs. angle of attack (α) for baseline and modified model with small sized (5S) SSVG.

3.3. Influence of 5M Type SSVG at Various Chordwise Locations (x/C)

To examine the variations of aerodynamic lift coefficients (C_L) of the 5M type SSVG, which was comparably larger than the 5S type, aerodynamic force measurements were performed. Additionally, experiments were also performed over the baseline clean wing configuration and the modified wing model blended with conventional rectangular VG to facilitate comparison of the results. All the test models were experimentally investigated for a wide range of angles of attack ($0^\circ < \alpha < 24^\circ$) at $Re = 2.0 \times 10^5$, as discussed in the preceding

section. The influence of 5M type SSVG at various chord locations was also included by blending the SSVG at three chordwise locations, namely 0.3C, 0.5C, and 0.8C. Figure 12 represents the variation of aerodynamic lift coefficients of all the test models as a function of the angle of attack (α). The difference in the lift coefficient plots (C_L) between the baseline clean wing configuration and the modified models blended with SSVG is evident from Figure 12 as it indicates that SSVG had some influence on the aerodynamic characteristics. As can be seen from Figure 12, in the case of baseline clean wing configuration the lift coefficient increases linearly along with the angle of attack till it reaches the vicinity of $\alpha = 6^\circ$. This area is called the linear region. After that, beyond $\alpha = 9^\circ$, the lift coefficient indicated a maximum value and then decreased due to the stall phenomenon. However, in the case of 5M type SSVG and the conventional rectangular VG, the lift coefficient was significantly reduced compared to the baseline clean wing configuration. The lift coefficient of 5M @ 0.3C was worse than the 5M @ 0.5C and 5M @ 0.8C configurations, and even poorer than the modified model blended with the conventional rectangular VG. For all the test models considered, the post-stall region's lift coefficient remained nearly consistent, with very small fluctuations between $15^\circ < \alpha < 24^\circ$. Even though the maximum lift coefficient (C_{Lmax}) of the baseline clean wing configuration was 5.70% greater than the modified models blended with SSVG, with a past stall angle at $\alpha = 12^\circ$ and the highest α , the baseline clean wing model showed marginally lower (C_L) than the modified models blended with SSVG. Therefore, it can be considered that the 5M type of SSVGs did not show any performance enhancements in terms of the lift characteristics curve, except at $\alpha = 12^\circ$ and at the highest α . The reduction in the maximum lift coefficient (C_{Lmax}) was most likely caused by the alternate flow pattern induced between the SSVG, i.e., the separated turbulent boundary layer arising out of the SSVG experiences a partial slip condition while in general, the airfoil surface without SSVG experienced a slip condition. Although this bi-periodic local pressure gradient, resulting in a spanwise flow energizing the flow, keeps the flow attached to the surface, it reduces the overall favorable pressure gradient between the upper and the lower surface of an airfoil. From this, it can be proposed that the decrease in the coefficient of lift (C_L) can be attributed to that local spanwise flow induced by the SSVG. Moreover, the results also indicate that the location in which the SSVGs are placed plays a vital role in determining the aerodynamic characteristics of that airfoil; as 5M @ 0.8C exhibited almost the same behavior as the baseline clean wing configuration, especially between $9^\circ < \alpha < 24^\circ$. Furthermore, it can be stated that when the SSVGs were blended over the test airfoil near the point of flow separation, the separated turbulent boundary layer generated by the SSVG induced a three-dimensional spanwise flow, thereby re-energizing the flow and helping to mitigate the flow separation. However, when the same SSVGs are placed before the point of separation, they tend to disturb more of the oncoming free stream flow, exhibiting detrimental effects. Furthermore, it should, however, be noted that no significant improvement in stall delay characteristics could be observed over the airfoil when the 5M type SSVG was utilized, whereas a 3° delay in a stall angle could be observed for the modified model blended with conventional rectangular VG. Overall the comparison of both the baseline and the modified model with 5M type SSVG blended at different chordwise locations showed no primary benefit, both in terms of maximum lift coefficient (C_{Lmax}) and delayed in the stall angle.

The drag coefficient curves for all the test models were plotted against the angle of attack (α), as shown in Figure 13. At low angles of attack (α), the modified models with SSVG showed a drag coefficient (C_D) modestly greater than the baseline clean wing model and the modified model blended with rectangular VG. The trend line of the characteristic drag coefficient (C_D) increased linearly against the angle of attack for the modified models with SSVG compared to other test models, as described in the previous section. Out of all the 5M type SSVG cases, the largest drag coefficient (C_D) at any angle belongs to the modified model with 5M @ 0.3C SSVG. However, out of all the test models, it becomes clear that the modified model blended with conventional rectangular VG had the highest drag coefficient (C_D) between $9^\circ < \alpha < 24^\circ$, except at $\alpha = 12^\circ$. On the contrary, 5M @ 0.5C

exhibited the lowest drag coefficient (C_D) between $12^\circ < \alpha < 24^\circ$, except at $\alpha = 15^\circ$ and in the pre-stall angles. It is clear from Figure 13 that beyond $\alpha = 9^\circ$, 5M @ 0.5C showed a relatively lesser drag coefficient than all the other test models. This marginal reduction in the drag coefficient (C_D) for 5M @ 0.5C can be attributed to the reattachment of the flow energized by SSVG through momentum transfer. However, the separated turbulent boundary layer significantly influenced the pressure drag on the surface.

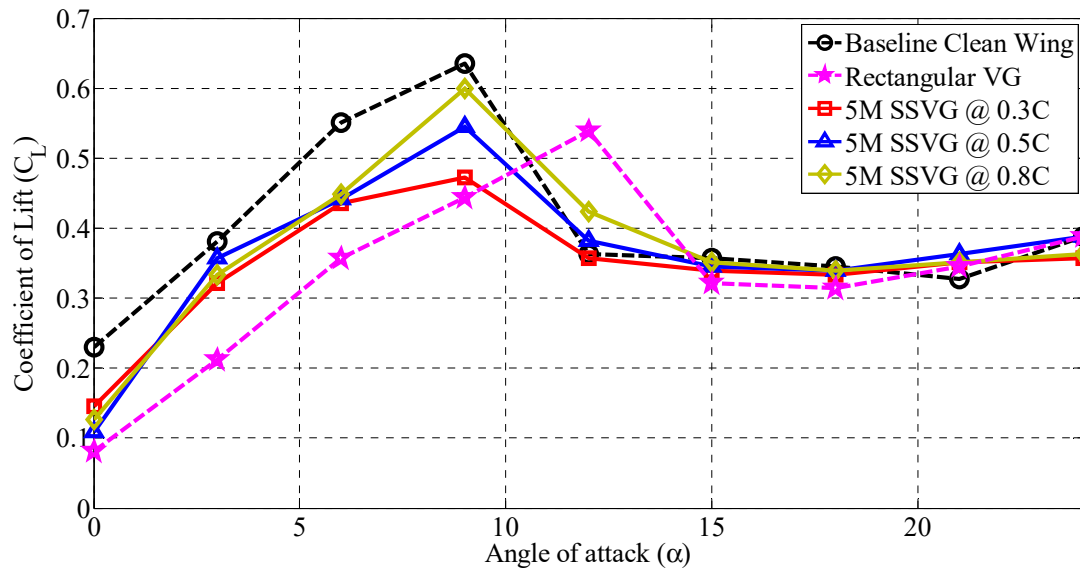


Figure 12. Coefficient of lift (C_L) vs. angle of attack (α) for the baseline and modified model with medium-sized (5M) shark scale vortex generators (SSVG).

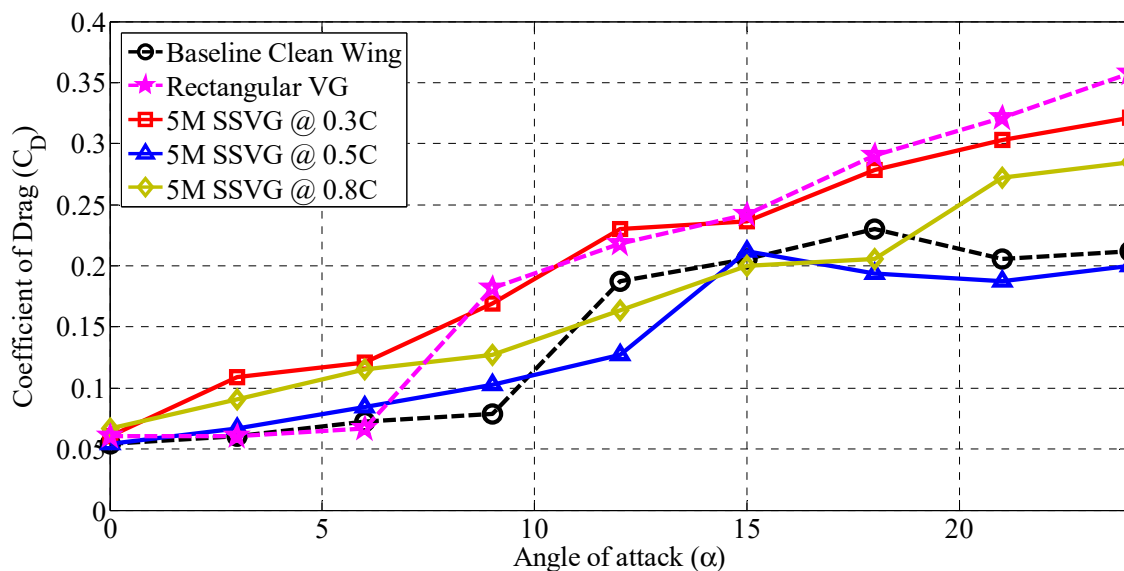


Figure 13. Coefficient of drag (C_D) vs. angle of attack (α) for the baseline and modified model with medium-sized (5M) shark scale vortex generators (SSVG).

3.4. Influence of 5L Type SSVG at Various Chordwise Locations (x/C)

Figure 14 represents the variations of the lift coefficient (C_L) against the angle of attack (α) for the baseline clean wing configuration and the modified models blended with rectangular VG and SSVG. To compare the effects of the 5L type SSVG at various chordwise locations, the relative lift and drag ratios were investigated in this section. The terms

“relative lift ratio” and “relative drag ratio” represent the lift and drag of the modified model divided by the lift and drag of the baseline model, respectively.

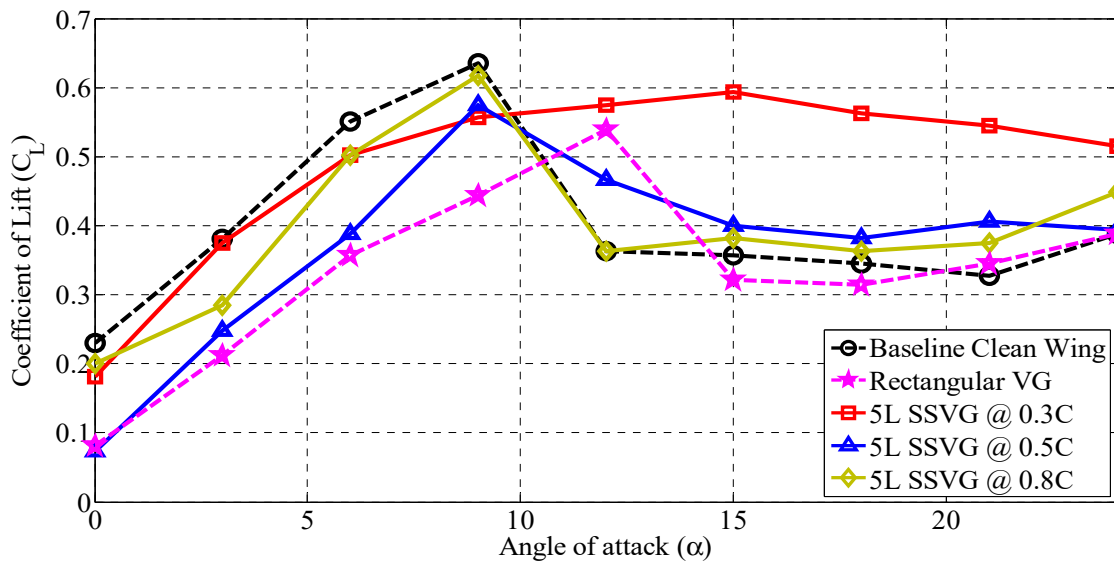


Figure 14. Coefficient of lift (C_L) vs. angle of attack (α) for baseline and modified model with large-sized (5L) shark scale vortex generators (SSVG).

$$\text{Relative lift ratio} = \frac{C_L \text{ of the modified model}}{C_L \text{ of the baseline model}} \quad (3)$$

$$\text{Relative drag ratio} = \frac{C_D \text{ of the modified model}}{C_D \text{ of the baseline model}} \quad (4)$$

The relative lift ratios for the baseline clean wing configurations and the modified models blended with rectangular VG and SSVG are presented in Figure 15. To ascertain good performance, a relative lift ratio of more than one and a relative drag ratio of less than one are desirable. It can be seen from Figure 15 that the modified models with 5L type SSVG performed well in the post-stall angles. However, in the pre-stall angle, the relative lift ratios were less than 1, indicating a decrease in the performance. The absence of lift enhancement in the pre-stall region followed by the optimum aerodynamic performance in the post-stall region indicates a qualitative change in the surface flow over the modified models relative to the baseline model due to the presence of SSVG. These results can be further supported by the hypothesis made by Lang et al. [15], that the shark scales are ineffective in mitigating the flow separation and postponing the point of separation until the angle of attack is beyond 12° .

The variations of the drag coefficient (C_D) vs. angle of attack (α) and the corresponding relative drag ratios are shown in Figures 16 and 17, respectively. The relative drag ratios of almost all the modified models with SSVG exhibited a greater relative drag ratio when compared against the baseline model, except 5L @ 0.5C between $12^\circ < \alpha < 18^\circ$. In the pre-stall angles of attack (α), the modified models with 5L type SSVG had crossed the value of 1, depicting a modestly greater relative drag when compared against the baseline model without SSVG. In addition to this, it was observed that placing the 5L type SSVG near the vicinity of the leading-edge tends to generate more drag, indicating that blending such SSVG at 0.3C would not offer any potential aerodynamic benefits, as discussed in the previous section. Moreover, the variation of the relative drag ratio of the modified models blended with SSVG to the baseline model seemed relatively small in terms of post-stall angles. It is noteworthy that the modified model blended with 5L type SSVG produced relatively lower drag than the conventional rectangular VG. However, the drastic increase observed in the relative drag ratio for the modified model blended with 5L type

SSVG was believed to be caused by the additional turbulent boundary layer induced by the SSVG in the flow fields in the form of vortices. The results indicate that, like the 5M type SSVGs, the 5L type SSVGs did not experience any stall delay characteristics. Understanding the underlying flow mechanism of the SSVG can help aerodynamic designers and engineers effectively engineer the flow field over the airfoil, aiming at achieving the optimum aerodynamic performance. It can also act as a guideline in administering the SSVG to effectively control the flow and mitigate the flow separation over the airfoil. The aerodynamic efficiency (L/D) ratio for the baseline and the modified model with SSVG presented in Figure 18 also represents the same. Not only did the modified model with SSVG show a lower lift curve slope in the pre-stall region, but also a lower lift coefficient (C_L) in the pre-stall region. On the other hand, in the post-stall angles, the modified model with SSVG exhibited a greater increase in the (C_L) when compared against the baseline model, resulting in an increased aerodynamic efficiency (L/D) between $12^\circ < \alpha < 24^\circ$. The lift to drag plot revealed that the baseline clean wing model maintained a larger L/D for angles of attack up to $\alpha = 12^\circ$. In contrast, the reduction in the aerodynamic efficiency (L/D) for the modified models blended with rectangular VG and bio-inspired SSVG can be attributed to the reduction in the overall favorable pressure gradient, resulting from the spanwise variation of the flow. However, in the post-stall angles, the separated turbulent boundary layer, in the form of vortices arising from the SSVG, imparted momentum to the flow, and offers aerodynamic benefits. Consequently, it can be claimed that the modified models with SSVG tends to be more aerodynamically efficient at post-stall angles. Moreover, the L/D plots indicate that the modified models blended with SSVG offered better aerodynamic efficiency when compared against the conventional rectangular VGs between $6^\circ < \alpha < 24^\circ$, except at $\alpha = 12^\circ$.

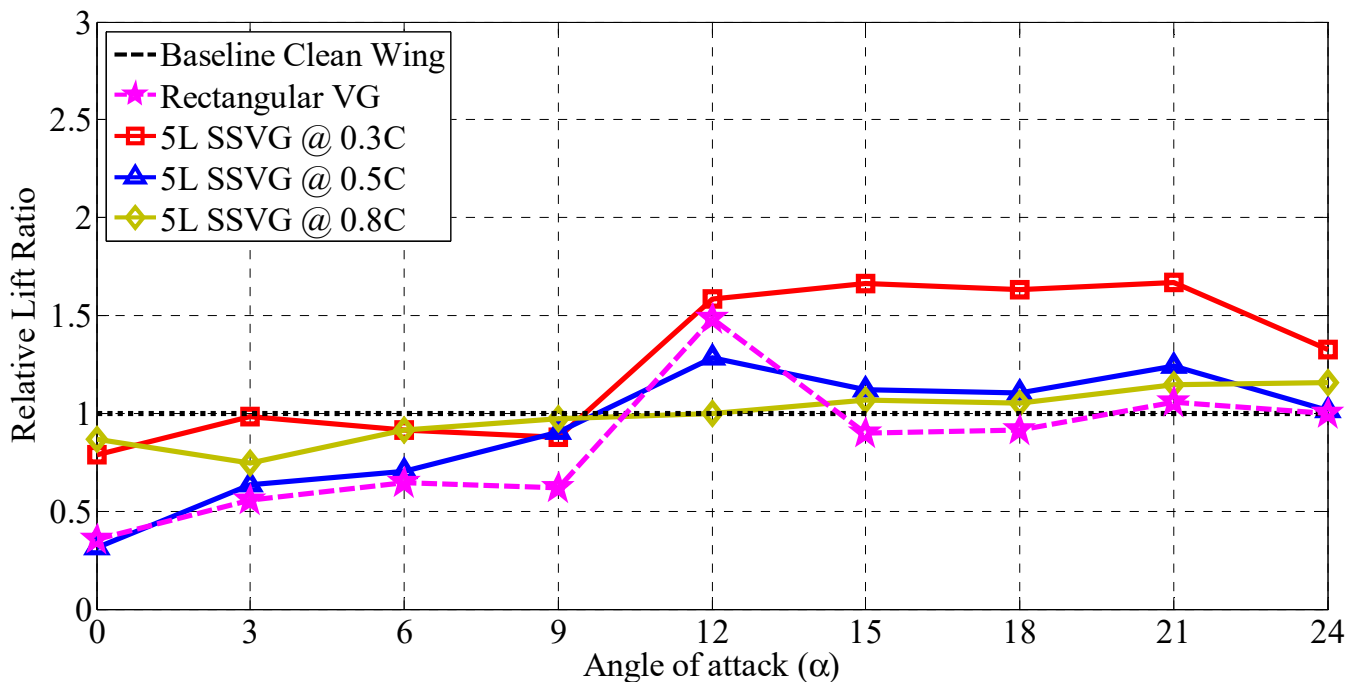


Figure 15. Relative lift ratio vs. angle of attack (α) for baseline and modified model for large-sized (5L) SSVG.

3.5. Understanding the Optimum Configuration of Modified Models with SSVG

A comparison of the aerodynamic forces like the coefficient of lift (C_L) and coefficient of drag (C_D) for the baseline clean wing configuration, modified model blended with rectangular VG, and modified model blended with three different sets of SSVG at various chordwise locations (x/C) is shown in Figures 19 and 20, respectively.

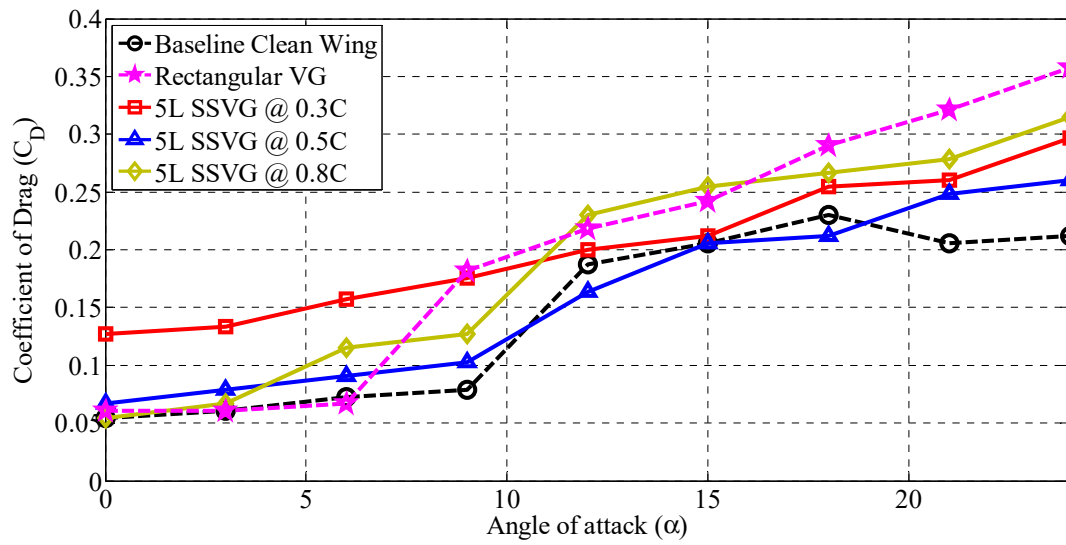


Figure 16. Coefficient of drag (C_D) vs. angle of attack (α) for baseline and modified model with large-sized (5L) SSVG.

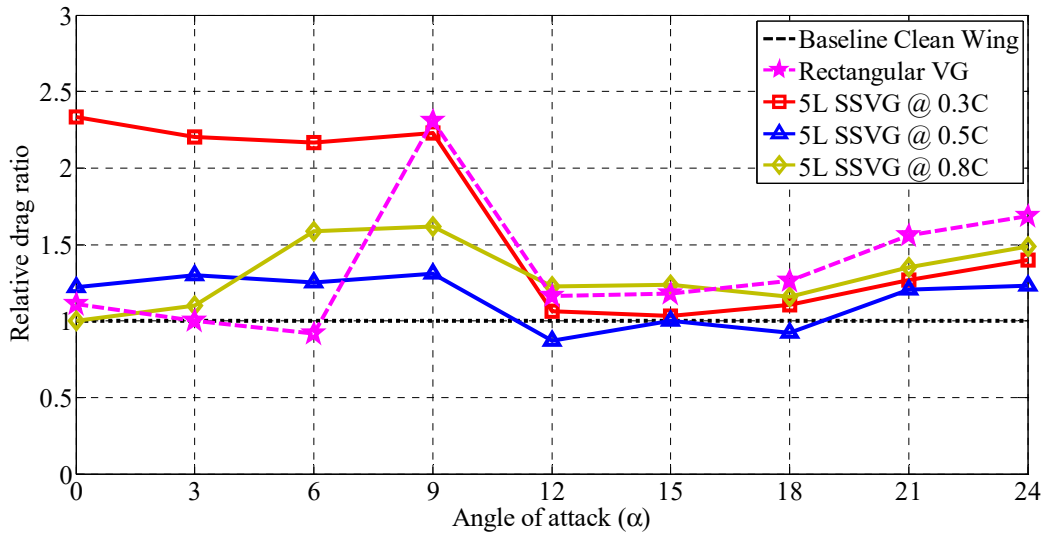


Figure 17. Relative drag ratio vs. angle of attack (α) for baseline and modified model with large-sized (5L) SSVG.

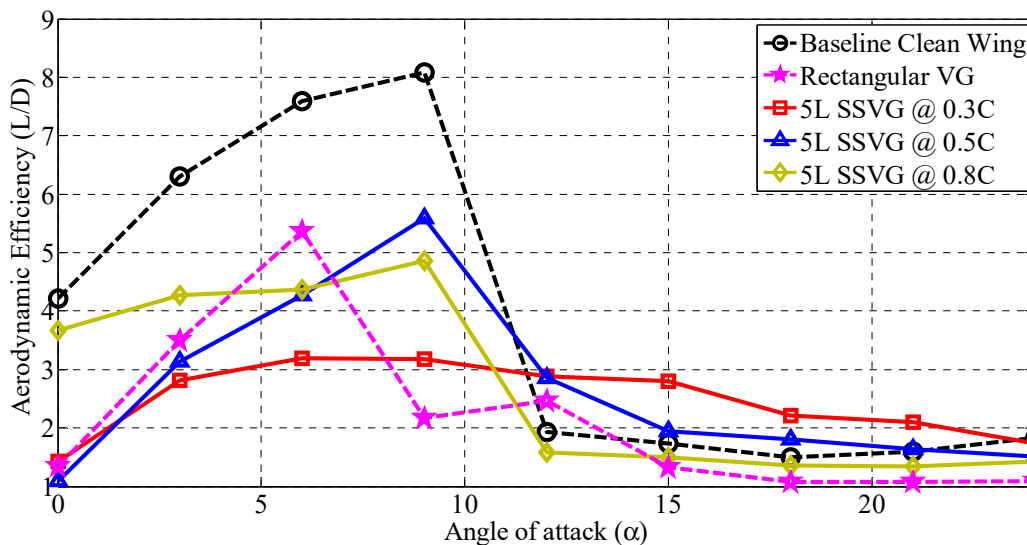


Figure 18. Aerodynamic efficiency (L/D) vs. (α) for baseline and modified model with large-sized (5L) SSVG.

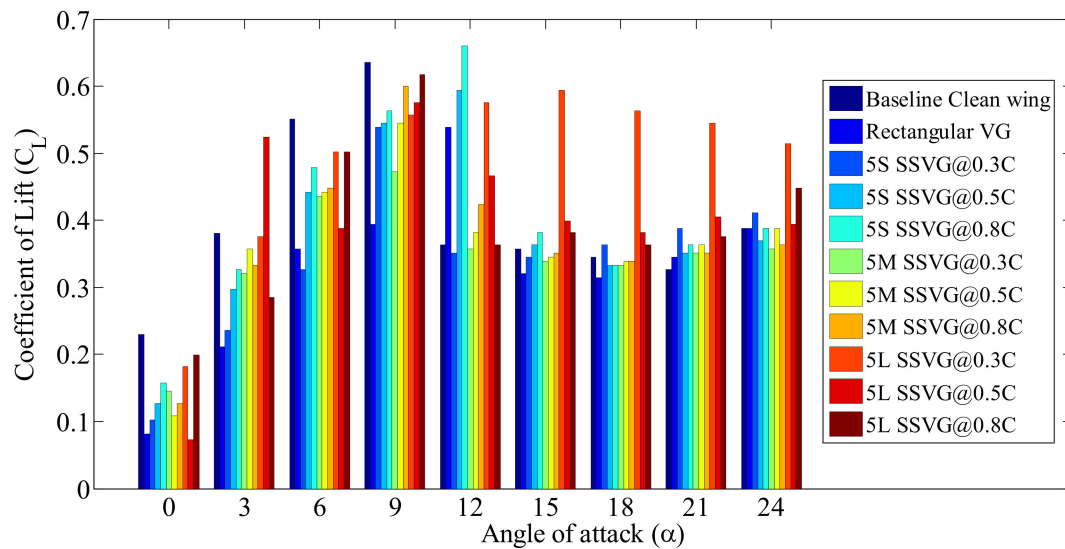


Figure 19. Comparison of the coefficient of lift (C_L) over baseline and modified wings with 5S, 5M, and 5L SSVG at various chordwise locations.

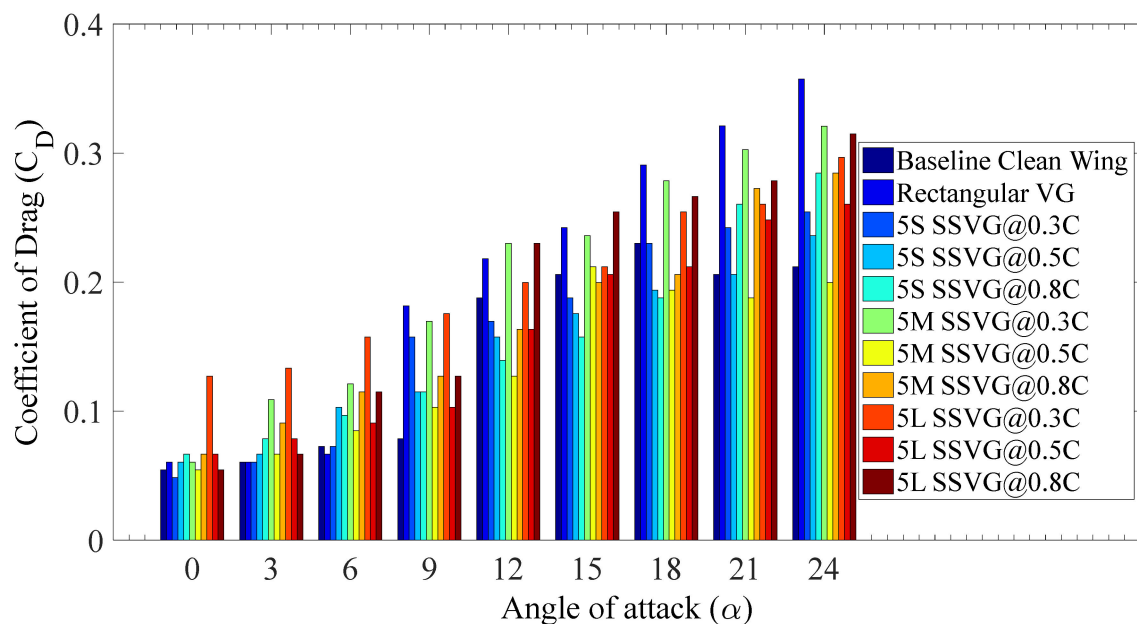


Figure 20. Comparison of the coefficient of drag (C_D) over baseline and modified wings with 5S, 5M, and 5L SSVG at various chordwise locations.

It is clear from the plots that in the post-stall angle, the characteristic lift coefficient (C_L) of the modified model blended with SSVG outperformed both the baseline clean wing configuration and the modified model blended with rectangular VGs. The 5L @ 0.3C exhibited the maximum lift coefficient throughout the post-stall angle $12^\circ < \alpha < 24^\circ$, except at $\alpha = 12^\circ$, where 5S @ 0.8C holds the C_{Lmax} . Even though the baseline clean wing configuration held the maximum lift coefficient value throughout the pre-stall regime, the results indicate that out of both the conventional rectangular VG and the bio-inspired SSVG cases, the 5L @ 0.3C showed better lift characteristics in both the pre-stall and the post-stall angles, except at $\alpha = 9^\circ$. Moreover, 5L @ 0.3C did not show any stall delay characteristics. In contrast to the 5L type SSVG @ 0.3C, another modified configuration, namely 5S @ 0.8C, offered the best aerodynamic benefits, like maximum lift coefficient (C_{Lmax}) associated with stall delay characteristics. The maximum lift coefficient (C_{Lmax}) of the baseline airfoil

was 0.63, whereas the modified model with SSVG 5S @ 0.8C showed a C_{Lmax} of 0.66, which was 3.80% greater than the baseline model. The result is in good agreement with Bechert et al. [14], who claimed that utilization of shark scales improved aerodynamic performance by 3%. Additionally, 5S @ 0.8C also offered benefits in terms of stall delay characteristics. The coefficient of lift (C_L) of the baseline model increased linearly till $\alpha = 9^\circ$, and then encountered stall, whereas the modified model 5S @ 0.8C stalled at $\alpha = 12^\circ$. Therefore, based on the experimental results, it can be concluded that the 5S type SSVG blended at 0.8C offered better aerodynamic benefits relative to the baseline clean wing model, modified model blended with rectangular VG, and its other SSVG counterparts. Similarly, the 5S type SSVG when located at 0.5C exhibited the minimum drag coefficient (C_D). Comparisons of the aerodynamic efficiency (L/D) of the baseline smooth wing and modified wings with conventional rectangular vortex generators, modified 5S, 5M, and 5L bio-inspired shark scale vortex generators are presented in Figure 21. Based on the experimental results, it was identified that each set of shark scale vortex generators yields a unique aerodynamic benefit in terms of (C_{Lmax}), C_{Dmin} , and stall delay, as shown in Table 3. Since the present work is the first of its kind, certain discrepancies in the aerodynamic force coefficients, i.e., C_{Lmax} , C_{Dmin} , etc., were found with the difference in the size of the SSVG. Henceforth, a deeper understanding of the underlying flow physics is deemed essential. Accordingly, the bristling angle selection needs to be considered since shark scales utilize bristling to mitigate the flow separation over the surface effectively.

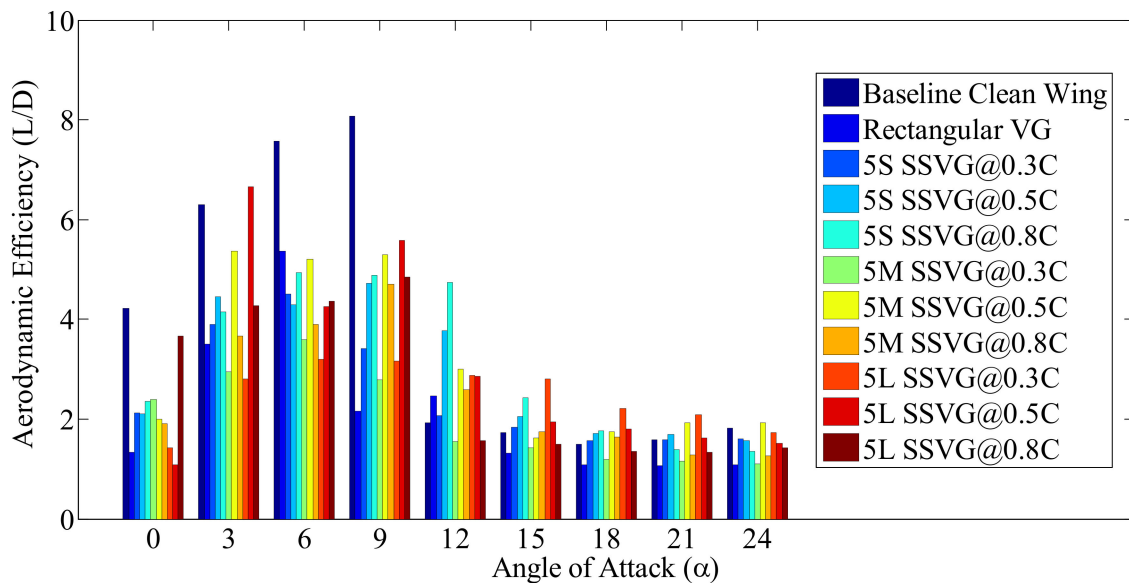


Figure 21. Comparison of aerodynamic efficiency (L/D) over baseline and modified wing with RVG, 5S, 5M, and 5L vortex generators.

Table 3. Optimum aerodynamic configurations of SSVG operating at $Re = 2.0 \times 10^5$.

Label	Parameter	Baseline	Modified	Benefits
5S@0.8C	C_{Lmax}	0.63	0.66	3.80% C_L increment
5S@0.8C	α at C_{Lmax}	9°	12°	Extended operating range
5S@0.3C	C_{Dmin}	0.05	0.04	Maximum drag reduction by 20%
5S@0.8C	α_{stall} , degree	9°	12°	Stall delay by 3°

4. Conclusions

In this study, the effectiveness of shark scale inspired vortex generators (SSVG) over the test airfoils at various chordwise locations (x/C) was investigated in a wide range of angles of attack (α), ranging from 0° to 24° , and in increments of 3° at $Re = 2.0 \times 10^5$. The

aerodynamic force measurements were obtained using a three-component force balance set up and a wind tunnel. Based on the experimental observations, the influence of the shark scale-based bio-inspired vortex generators (SSVG) on the aerodynamic characteristics of the airfoil were studied in detail and the following conclusions were made:

1. Incorporation of the 5S type SSVG at 0.8C chordwise distance of the airfoil enhance the lift coefficient (C_L) by about 3.80% when compared against the baseline NACA 0015 airfoil model.
2. 5S type SSVG, when placed at 0.8C, showed that it is effective in delaying the stall by effectively mitigating the flow separation.
3. Shark scale-inspired vortex generators of 5S type, when installed at 0.3C, exhibits the lowest drag coefficient (C_D) when compared against the baseline model.
4. Shark scale-inspired vortex generators of the 5S type, when installed at 0.5C and 0.8C, offered better aerodynamic characteristics relative to the conventional rectangular VG.

The experimental results showed that bio-inspired shark scale vortex generators (SSVG) could delay stall characteristics and help reducing the adverse effects of flow separation. This research can be further extended to consider the impact of bristling angle, Reynolds number, etc., with in the scope for future research, before looking for practical applications. Likewise, surface pressure over the airfoil models featuring SSVG can be studied to better understand the underlying flow physics. Optimization studies involving genetic algorithms might further improve the effectiveness of the SSVG applications over the airfoil.

Author Contributions: Conceptualization, S.N.P., writing—original draft preparation, S.A., V.S.R., S.N.P.; project administration, S.N.P. and A.A.P.; writing, review, and editing, A.A.P., M.M.R., and K.A.J.; supervision, S.N.P. and funding acquisition, A.A.P. All authors have read and agreed to the published version of the manuscript.

Funding: This project was funded by the Deanship of Scientific Research (DSR), King Abdulaziz University, Jeddah, under grant No. (DF-359-135-1441). The authors, therefore, gratefully acknowledge DSR technical and financial support.

Conflicts of Interest: The authors declare no conflict of interest.

Abbreviations

SSVG	Shark Scale Vortex Generator
VG	Vortex Generator
Re	Reynolds number
β	Bristling angle
UAV	Unmanned Aerial Vehicle
MAV	Micro Aerial Vehicle
NACA	National Advisory Committee for Aeronautics
A	Amplitude (in mm)
λ	Wavelength (in mm)
c	Chordlength (in mm)
b	Span (in mm)
PLA	Poly lactic acid (or) Polylactide
MPS	Miniature Pressure Scanner
F_L	Lift force
F_D	Drag force
C_L	Coefficient of lift
C_{Lmax}	Maximum coefficient of lift
C_D	Coefficient of drag
C_{Dmin}	Minimum coefficient of drag
L/D	Aerodynamic efficiency
ρ	Density of fluid

v	Free-stream velocity
s	Wing area
$dC_L/d\alpha$	Lift curve slope
α	Angle of attack
α_{stall}	Stalling angle of attack
x/C	Chordwise location

References

- Choi, H.; Park, H.; Sagong, W.; Lee, S. Biomimetic flow control based on morphological features of living creatures. *Phys. Fluids* **2012**, *24*. [[CrossRef](#)]
- Feld, K.; Kolborg, A.N.; Nyborg, C.M.; Salewski, M.; Steffensen, J.F.; Berg-Sørensen, K. Dermal denticles of three slowly swimming shark species: Microscopy and flow visualization. *Biomimetics* **2019**, *4*, 38. [[CrossRef](#)]
- Raheem, M.A.; Edi, P.; Pasha, A.A.; Rahman, M.M.; Juhany, K. Numerical Study of Variable Camber Continuous Trailing Edge Flap at Off-Design Conditions. *Energies* **2019**, *12*, 3185. [[CrossRef](#)]
- Popp, M.; White, C.F.; Bernal, D.; Wainwright, D.K.; Lauder, G.V. The denticle surface of thresher shark tails: Three-dimensional structure and comparison to other pelagic species. *J. Morphol.* **2020**, *281*, 938–955. [[CrossRef](#)]
- Domel, A.G.; Saadat, M.; Weaver, J.C.; Haj-Hariri, H.; Bertoldi, K.; Lauder, G.V. Shark skin-inspired designs that improve aerodynamic performance. *J. R. Soc. Interface* **2018**, *15*. [[CrossRef](#)]
- Sudin, M.N.; Abdullah, M.A.; Shamsuddin, S.A.; Ramli, F.R.; Tahir, M.M. Review of research on vehicles aerodynamic drag reduction methods. *Int. J. Mech. Mechatron. Eng.* **2014**, *14*, 35–47.
- Bar-Cohen, Y. Introduction to Biomimetics: The Wealth of Inventions in Nature as an Inspiration for Human Innovation. In *Biomimetics: Biologically Inspired Technologies*; CRC Press: Boca Raton, FL, USA, 2006.
- Camhi, M.D.; Pikitch, E.K.; Babcock, E.A. *Sharks of the Open Ocean: Biology, Fisheries and Conservation*; Wiley: Hoboken, NJ, USA, 2009; p. 502. [[CrossRef](#)]
- Videler, J.J. Body surface adaptations to boundary-layer dynamics. *Symp. Soc. Exp. Biol.* **1995**, *49*, 1–20. [[PubMed](#)]
- Patricia, F.W.; Guzman, D.; Iñigo, B.; Urtzi, I.; Maria, B.J.; Manu, S. Morphological Characterization and Hydrodynamic Behavior of Shortfin Mako Shark (*Isurus oxyrinchus*) Dorsal Fin Denticles. *J. Bionic Eng.* **2019**, *16*, 730–741. [[CrossRef](#)]
- Lang, A.W.; Hidalgo, P. Cavity Flow Characterization of the Bristled Shark Skin Microgeometry. In Proceedings of the 47th AIAA Aerospace Sciences Meeting including the New Horizons Forum and Aerospace Exposition, Orlando, FL, USA, 5–8 January 2009.
- Motta, P.; Habegger, M.L.; Lang, A.; Hueter, R.; Davis, J. Scale morphology and flexibility in the shortfin mako *Isurus oxyrinchus* and the blacktip shark *Carcharhinus limbatus*. *J. Morphol.* **2012**, *273*, 1096–1110. [[CrossRef](#)]
- Lang, A.; Motta, P.; Habegger, M.L.; Hueter, R.; Afroz, F. Shark skin separation control mechanisms. *Mar. Technol. Soc. J.* **2011**, *45*, 208–215. [[CrossRef](#)]
- Bechert, D.W.; Bruse, M.; Hage, W.; Meyer, R. Fluid mechanics of biological surfaces and their technological application. *Naturwissenschaften* **2000**, *87*, 157–171. [[CrossRef](#)]
- Lang, A.W.; Bradshaw, M.T.; Smith, J.A.; Wheelus, J.N.; Motta, P.J.; Habegger, M.L.; Hueter, R.E. Movable shark scales act as a passive dynamic micro-roughness to control flow separation. *Bioinspiration Biomim.* **2014**, *9*. [[CrossRef](#)] [[PubMed](#)]
- Zhen, T.K.; Zubair, M.; Ahmad, K.A. Experimental and numerical investigation of the effects of passive vortex generators on Aludra UAV performance. *Chin. J. Aeronaut.* **2011**, *24*, 577–583. [[CrossRef](#)]
- Ashill, P.R.; Fulker, J.L.; Hackett, K.C. A review of recent developments in flow control. *Aeronaut. J.* **2005**, *109*, 205–232. [[CrossRef](#)]
- Lin, J.C. Review of research on low-profile vortex generators to control boundary-layer separation. *Prog. Aerosp. Sci.* **2002**, *38*, 389–420. [[CrossRef](#)]
- Fouatih, O.M.; Medale, M.; Imine, O.; Imine, B. Design optimization of the aerodynamic passive flow control on NACA 4415 airfoil using vortex generators. *Eur. J. Mech.-B/Fluids* **2016**, *56*, 82–96. [[CrossRef](#)]
- Wang, H.; Zhang, B.; Qiu, Q.; Xu, X. Flow control on the NREL S809 wind turbine airfoil using vortex generators. *Energy* **2017**, *118*, 1210–1221. [[CrossRef](#)]
- Zhi-yong, Z.; Wang-long, Z.; Zhi-hua, C.; Xiao-hui, S.; Chen-chao, X. Suction control of flow separation of a low-aspect-ratio wing at a low Reynolds number. *Fluid Dyn. Res.* **2018**, *50*, 065504. [[CrossRef](#)]
- Yousefi, K.; Saleh, R. Three-dimensional suction flow control and suction jet length optimization of NACA 0012 wing. *Meccanica* **2015**, *50*, 1481–1494. [[CrossRef](#)]
- You, D.; Moin, P. *Active Control of Flow Separation Over an Airfoil Using Synthetic Jets*, In *Solid Mechanics and Its Applications*; Springer Verlag: Heidelberg, Germany, 2009; Volume 14, pp. 551–561.
- Minelli, G.; Hartono, E.A.; Chernoray, V.; Hjelm, L.; Krajnović, S. Aerodynamic flow control for a generic truck cabin using synthetic jets. *J. Wind Eng. Ind. Aerodyn.* **2017**, *168*, 81–90. [[CrossRef](#)]
- Greenblatt, D.; Wygnanski, I.J. The Control of flow separation by periodic excitation. *Prog. Aerosp. Sci.* **2000**, *36*, 487–545. [[CrossRef](#)]
- Brunn, A.; Nitsche, W. Separation Control in an Axisymmetric Diffuser Flow by Periodic Excitation. In *Engineering Turbulence Modelling and Experiments 5*; Rodi, W., Fueyo, N., Eds.; Elsevier Science Ltd.: Oxford, UK, 2002; pp. 587–596; ISBN 978-0-08-044114-6.

27. Yousefi, K.; Saleh, R. The effects of trailing edge blowing on aerodynamic characteristics of the naca 0012 airfoil and optimization of the blowing slot geometry. *J. Theor. Appl. Mech.* **2014**, *52*, 165–179. [[CrossRef](#)]
28. Ganesh, N.; Arunvinthan, S.; Pillai, S. Effect of surface blowing on aerodynamic characteristics of tubercled straight wing. *Chin. J. Aeronaut.* **2019**, *32*, 1111–1120. [[CrossRef](#)]
29. Raayai-Ardakani, S.; McKinley, G.H. Drag reduction using wrinkled surfaces in high Reynolds number laminar boundary layer flows. *Phys. Fluids* **2017**, *29*. [[CrossRef](#)]
30. Raayai-Ardakani, S.; McKinley, G.H. Geometric optimization of riblet-textured surfaces for drag reduction in laminar boundary layer flows. *Phys. Fluids* **2019**, *31*. [[CrossRef](#)]
31. Zhang, Y.; Yan, C.; Chen, H.; Yin, Y. Study of riblet drag reduction for an infinite span wing with different sweep angles. *Chin. J. Aeronaut.* **2020**, *33*, 3125–3137. [[CrossRef](#)]
32. Ismail, M.F.; Vijayaraghavan, K. The effects of aerofoil profile modification on a vertical axis wind turbine performance. *Energy* **2015**, *80*, 20–31. [[CrossRef](#)]
33. Jones, G.; Santer, M.; Debiassi, M.; Papadakis, G. Control of flow separation around an airfoil at low Reynolds numbers using periodic surface morphing. *J. Fluids Struct.* **2018**, *76*, 536–557. [[CrossRef](#)]
34. Luo, H.; Qiao, W.; Xu, K. Passive control of laminar separation bubble with spanwise groove on a low-speed highly loaded low-pressure turbine blade. *J. Therm. Sci.* **2009**, *18*, 193–201. [[CrossRef](#)]
35. Seo, S.-H.; Hong, C.-H. Performance improvement of airfoils for wind blade with the groove. *Int. J. Green Energy* **2015**, *13*, 34–39. [[CrossRef](#)]
36. Law, Y.Z.; Jaiman, R.K. Passive control of vortex-induced vibration by spanwise grooves. *J. Fluids Struct.* **2018**, *83*, 1–26. [[CrossRef](#)]
37. Mu, T.; Zhang, R.; Xu, H.; Zheng, Y.; Fei, Z.; Li, J. Study on improvement of hydraulic performance and internal flow pattern of the axial flow pump by groove flow control technology. *Renew. Energy* **2020**, *160*, 756–769. [[CrossRef](#)]
38. McAuliffe, B.R.; Yaras, M.I. Passive manipulation of separation-bubble transition using surface modifications. *J. Fluids Eng.* **2009**, *131*. [[CrossRef](#)]
39. D’Alessandro, V.; Clementi, G.; Giammichele, L.; Ricci, R. Assessment of the dimples as passive boundary layer control technique for laminar airfoils operating at wind turbine blades root region typical Reynolds numbers. *Energy* **2019**, *170*, 102–111. [[CrossRef](#)]
40. Robarge, T.W.; Stark, A.M.; Min, S.; Khalatov, A.A.; Byerley, A. Design Considerations for Using Indented Surface Treatments to Control Boundary Layer Separation. In Proceedings of the 42nd AIAA Aerospace Sciences Meeting and Exhibit, Reno, NV, USA, 5–8 January 2004; pp. 1–10.
41. Huang, L.; Huang, P.G.; LeBeau, R.P.; Hauser, T. Numerical study of blowing and suction control mechanism on NACA0012 airfoil. *J. Aircr.* **2004**, *41*, 1005–1013. [[CrossRef](#)]
42. Junxuan, C.; Xun, G.Z. Numerical study on drag reduction by micro-blowing/suction compounding flow control on supercritical airfoil. *Procedia Eng.* **2015**, *99*, 613–617. [[CrossRef](#)]
43. Akansu, Y.E.; Karakaya, F.; Şanlısoy, A. Active control of flow around NACA 0015 airfoil by using DBD plasma actuator. *EPJ Web Conf.* **2013**, *45*. [[CrossRef](#)]
44. Guoqiang, L.; Weiguo, Z.; Yubiao, J.; Pengyu, Y. Experimental investigation of dynamic stall flow control for wind turbine airfoils using a plasma actuator. *Energy* **2019**, *185*, 90–101. [[CrossRef](#)]
45. Arunvinthan, S.; Pillai, S.; Cao, S. Aerodynamic characteristics of variously modified leading-edge protuberanced (LEP) wind turbine blades under various turbulent intensities. *J. Wind Eng. Ind. Aerodyn.* **2020**, *202*, 104188. [[CrossRef](#)]
46. Zhang, Y.; Zhang, X.; Li, Y.; Chang, M.; Xu, J. Aerodynamic performance of a low-Reynolds UAV with leading-edge protuberances inspired by humpback whale flippers. *Chin. J. Aeronaut.* **2021**, *34*. [[CrossRef](#)]
47. Custodio, D.; Henocho, C.W.; Johari, H. Aerodynamic characteristics of finite span wings with leading-edge protuberances. *AIAA J.* **2015**, *53*, 1878–1893. [[CrossRef](#)]
48. Sicot, C.; Devinant, P.; Loyer, S.; Hureau, J. Rotational and turbulence effects on a wind turbine blade. Investigation of the stall mechanisms. *J. Wind Eng. Ind. Aerodyn.* **2008**, *96*, 1320–1331. [[CrossRef](#)]
49. Li, Q.; Maeda, T.; Kamada, Y.; Murata, J.; Furukawa, K.; Yamamoto, M. Effect of number of blades on aerodynamic forces on a straight-bladed Vertical Axis Wind Turbine. *Energy* **2015**, *90*, 784–795. [[CrossRef](#)]
50. Abohela, I.; Hamza, N.; Dudek, S. Effect of roof shape, wind direction, building height and urban configuration on the energy yield and positioning of roof mounted wind turbines. *Renew. Energy* **2013**, *50*, 1106–1118. [[CrossRef](#)]
51. Roach, P.E. The generation of nearly isotropic turbulence downstream of streamwise tube bundles. *Int. J. Heat Fluid Flow* **1986**, *7*, 117–125. [[CrossRef](#)]
52. Arunvinthan, S.; Pillai, S. Aerodynamic characteristics of unsymmetrical aerofoil at various turbulence intensities. *Chin. J. Aeronaut.* **2019**, *32*, 2395–2407. [[CrossRef](#)]